AWES2020
20th Australasian Wind Engineering Society Workshop
8 – 9 April, 2021

Single-Cell Buoyancy Vortex CFD Modelling

K.-W. Leong[1], M. MacDonald[1], J.E. Cater[2], R.G.J. Flay[1]
[1]*Department of Mechanical Engineering*
The University of Auckland, Auckland CBD 1010, New Zealand
[2]*Department of Engineering Science*
The University of Auckland, Auckland CBD 1010, New Zealand

ABSTRACT

This paper describes the process and preliminary results of a work-in-progress buoyancy vortex CFD model. A single-cell vortex was modelled in a wedge-shaped domain with inlet flow speeds ranging between 0.05 - 3 m/s at steady state conditions. The domain dimensions, heated plate temperatures of 105 °C and 135 °C, and the swirl vane angle of 30° were based on buoyancy vortex laboratory experiments conducted by Mullen and Maxworthy in 1977. The resultant flow model obtained using ANSYS-CFX was found to be similar to the flow structure obtained experimentally. The swirling flow transitioned from the boundary layer above the heated floor and angled vane into a vertical vortex and merged with the single-cell vortex above the plate. Mesh refinement and uncertainty analysis also revealed that the apparent order of convergence for the vortex temperature was 2.12 and average vorticity was 1.59 - 1.60, and that the estimated uncertainty of the vortex core temperature values above ambient at 300 mm height was no higher than 0.02 °C.

1. Introduction

Dust-devil buoyancy-induced vortices are formed when an air parcel is warmed by a hot ground surface and rises, combining swirl and vorticity that is created from the interactions between the ambient wind and the ground. Field measurements by Kaimal and Businger (1970) revealed that the kinetic and thermal energy fluxes in a dust-devil vortex were up to an order of magnitude higher than the counterparts in a non-spinning thermal plume that was formed under similar conditions. Given this potential, efforts are being made to harness the buoyancy vortex kinetic energy for electricity production (Glezer & Simpson, 2014; Nižetić, 2018). While the axial (vertical) pressure gradient is generated from buoyancy at the vortex core, swirl is generated when the friction imposed by the ground surface and ambient wind shear reduces the tangential velocity and centrifugal force, resulting in air being drawn into the vortex base by the radial pressure gradient (Hawkes & Flay, 2016; Stull, 2016).

A single-cell vortex is identified by updraft flow across the entire core. As the ratio of tangential velocity to radial velocity is increased (to increase fluid angular momentum on ground level) for a given heat input, helped by increasing the angle of the vertical guide vanes placed across the outer circumference of a buoyancy vortex chamber inlet (and leading to a decreased spacing between the adjacent vanes), a reduction in the rotation-induced pressure within the vortex core is obtained. There is also an increased axial pressure gradient along the vortex centreline, and the formation of a downdraft along the centreline which creates the second vortex cell (Fitzjarrald, 1973; Simpson & Glezer, 2016). This feature results in a temperature reduction in the vortex core compared to the surrounding zone (Mullen & Maxworthy, 1977, herein referred to as MM in capital letters).

CFD is applied to model the swirl flow characteristics of a buoyancy vortex arising from a reservoir of heat energy at ground level as it interacts with the ambient air parcel above. In the case of laboratory-scale buoyancy vortex generation through a heated plate placed at ground level, MM described the swirling vortex flow characteristics with the matching air temperature distributions across the chamber given various heat inputs and inlet flow angles across twelve directional flow vanes. An attempt has been made to model the buoyancy vortex flow structure as it reaches steady state in the vane-equipped vortex chamber using ANSYS-CFX 2020R1, with similar chamber and vane dimensions and heat input from the plate to the experimental work.

2. Methodology

2.1 CFD Modelling Domain

The present numerical domain models the experimental conditions described in MM. Even though MM reported that the vortex was not always axisymmetric and moved around in the experimental domain, the buoyancy vortex chamber was modelled as a 30° (360°/12) wedge domain across a single vane to reduce computational time and given that MM assumed axisymmetric conditions to average their vortex flow and temperature measurements. Match control and rotational periodic boundary condition were established across the two wedge faces to ensure that ANSYS-CFX would derive the effects of the remainder of the chamber (ANSYS, 2020). The vane (of height 1.83 m, width 150 mm and thickness 3.2 mm) was modelled within the domain at 30° with respect to the radial direction (Figure 1), given that the preliminary task was to model a single-cell vortex, which MM reported was created by setting the vane angle at 30°. The heated plate was set as a no-slip wall boundary, assumed to be isothermal and held at a constant temperature of either 105 °C or 135 °C to match the experimental heat inputs of 778 W and 1058 W respectively.

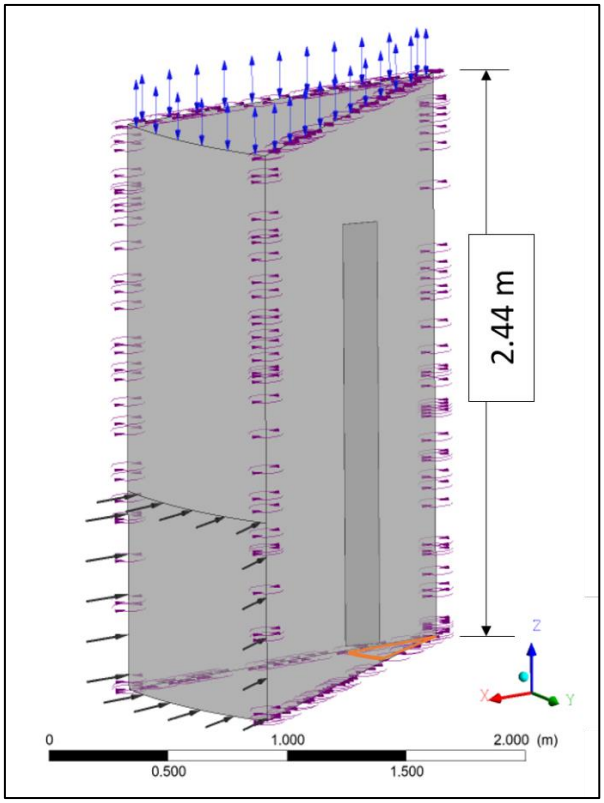

Figure 1. Model domain including heated plate (outlined in orange) and swirl vane. Flow inlet indicated in black arrows, the vortex outlet defined as an opening in ANSYS-CFX-Pre indicated in blue arrows, and the rotational periodic boundary conditions across the two wedge surfaces indicated in purple rotational arrows.

Air enters from the opening below the cylindrical chamber wall and the inlet velocity was defined in the form of a radial velocity component in cylindrical coordinates in a stationary frame of reference. Without an inlet velocity specified, a 0 Pa total pressure specified at the chamber entrance and an average 0 Pa static pressure specified at the chamber opening facing the ceiling led to ANSYS-CFX generating a heat soak condition, i.e., an elevated air temperature across the entire chamber.

A weak cross flow and perforated ceiling were incorporated at the top of the chamber during the experiments to minimise heat being trapped at the top of the chamber. However, no chamber outlet velocity profile or pressure data were reported. In the CFD, the chamber outlet facing the ceiling was deemed to be at atmospheric pressure with an average static pressure of 0 Pa. The chamber ceiling was defined as an opening.

2.2 CFD Numerical Method

The continuity, momentum and thermal energy equations were applied in a stationary frame of reference, with no external momentum source and negligible internal heating by fluid viscosity. The ANSYS-CFX "High Resolution" advection scheme was used, as it provides a nonlinear function to blend the central and first-order upwind differencing schemes to minimise the effects of the unphysical oscillations as well as false diffusion (ANSYS, 2020). The behaviour of the thermal boundary layer above the plate was reported to not be a strong function of the input heat energy and vane angle. The effect of thermal diffusion was thus deemed negligible. On the other hand, a large temperature gradient beyond the thermal boundary layer was reported, generated when the hot air rising from the plate was replaced by the cooler air directed by the vanes at an angle, which caused the flow to swirl over the heated plate. As the terms of order ΔT^2 or higher cannot be neglected due to the relatively large temperature gradients, the Boussinesq approximation, which defines the density at the local temperature T with respect to the ambient temperature $T\infty$ using a truncated Taylor series expansion (Moukalled et al., 2016), does not apply in this case. The flow across the modelled domain was driven by momentum through the imposed inlet velocity, and the temperature values used for the thermal energy equation are passive scalars. No initial inlet velocity value was reported in the experiments, but a unidirectional reference velocity of 0.05 - 3.0 m/s in the inwards radial direction was used as the initial boundary condition. Different simulations with the 0.05 m/s, 0.1 m/s, 0.2 m/s and 0.4 m/s inlet velocities were utilised for the 0.0322 m coarse meshes, and different simulations with the 0.1 m/s and 3.0 m/s inlet velocities were utilised for the 0.0150 m fine meshes.

The vortex flow was modelled as a turbulent flow at steady state (with inlet turbulence intensity set at 5%) given that the vortex core Reynolds number during the experiments ranged between $5 \times 10^3 - 1 \times 10^4$ when the mean vortex behaviour was recorded. The *k-ω* based shear-stress-transport (SST) model pioneered by Menter (1994) was utilised. For the turbulence model to work properly, an automatic inflation setting of 15 nodes or layers recommended by ANSYS was implemented on the vane, heated plate, floor and cylindrical chamber walls in the direction normal to the walls. For the vane walls, the automatic setting refined the boundary layer meshes only at the vane surface facing downstream (of the flow inlet direction) as the global mesh sizes were reduced. In the future, attempts should be made to refine the meshes that surround the other vane surfaces. The 0.0150 m fine mesh wedge domain consisted of 440,894 nodes, 1,513,632 tetrahedrons, 298,340 prisms and 2,202 pyramids. Convergence control was set with 1000 maximum iterations, and convergence criteria were set with residual type root-mean-square (RMS) and residual target at 1e-6.

3. Results and Discussion

3.1 Flow and Temperature Profile Comparison

Flow modelling was initially conducted with the flow inlet velocities between 0.05 - 0.4 m/s using the coarse 0.0322 m meshes to investigate the effect of the inlet flow rate on the buoyancy vortex temperature profile. From the air temperature distribution along the chamber central vertical axis, the CFX solver revealed that an increasing inlet radial velocity would ensure a greater amount of heat transfer by convection from the heated plate (Table 1). This is consistent with the general observation by MM that the hot air rising from the plate is replaced by the cooler air drawn into the vortex core.

Table 1. Effect of inlet flow velocity on buoyancy vortex temperature above ambient (ΔT) along chamber central vertical axis for 105 °C plate temperature. The model used a mesh spacing of 0.0322 m.

	Inlet radial velocity			
Height above heated plate axis	0.05 m/s	0.1 m/s	0.2 m/s	0.4 m/s
Z = 100 mm	67 °C	62 °C	52 °C	38 °C
Z = 300 mm	48 °C	33 °C	22 °C	16 °C
Z = 600 mm	25 °C	15 °C	10 °C	7 °C

Figure 2 shows that for both the 105 °C and 135 °C inputs and using the fine meshes, the vortex temperature profiles (where ΔT = temperature increase over ambient) obtained through modelling appear more parabolic whereas the counterparts obtained experimentally appear more exponential at 0 - 600 mm above the heated plate and its thermal boundary layer, with largely dissimilar modelled and experimental temperature values. Still, both sets of temperature profiles as well as the streamlines in Figure 3 near the vertical chamber axis 600 mm above the plate indicate a single-cell vortex core structure being formed, with the vane section facing the inlet directing the flow into a counter clockwise swirl direction viewed from above. The 1/12 segment plate area integral heat flux calculated by ANSYS-CFX for the 0.1 m/s inlet radial velocity was only approximately 6 W and 8 W compared to 65 W (105 °C plate, 778/12 W) and 88 W (135 °C plate, 1058/12 W) obtained experimentally, respectively. The inlet radial velocity had to be increased to 3.0 m/s in order to match the calculated heat flux with the experimental results: A modelled input heat flux of 65 W was used for the 105 °C plate and 89 W for the 135 °C plate, even though this would also result in a much lower modelled ΔT compared to the experimental counterparts (Table 1).

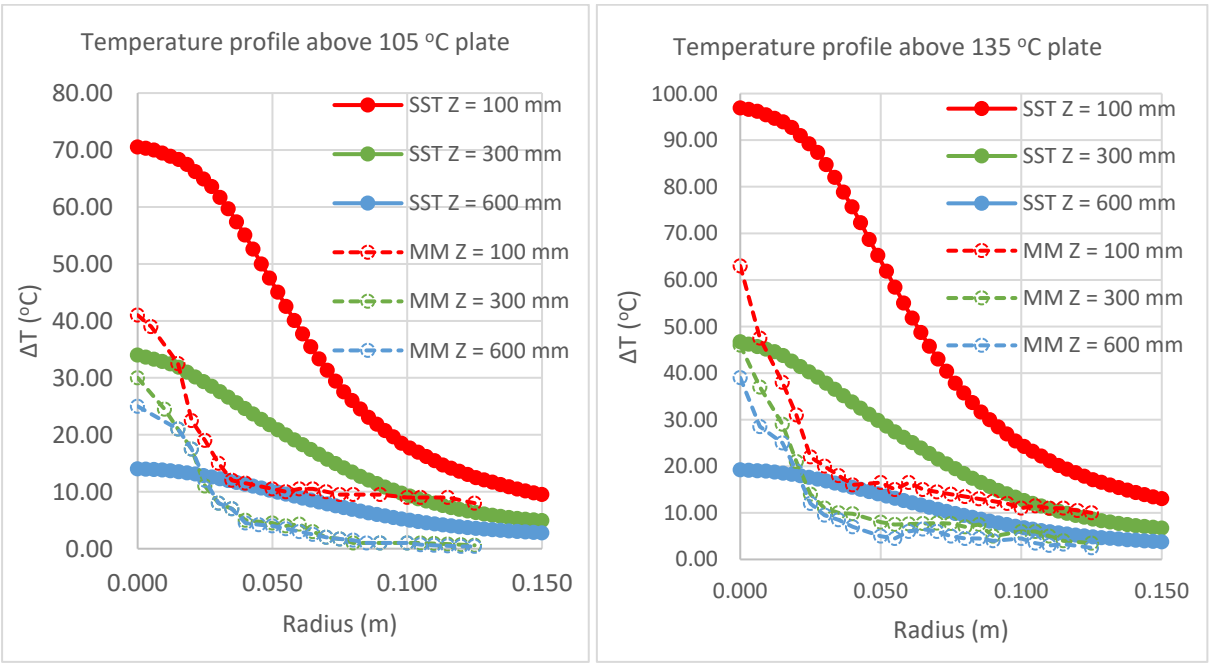

Figure 2. Azimuthally-averaged temperature profiles in a single-cell vortex at 100 mm, 300 mm and 600 mm above the thermal source in the experiment (MM) and modelled (SST) conditions, at 30° vane angle and 0.1 m/s inlet radial velocity. The model used a mesh spacing of 0.0150 m.

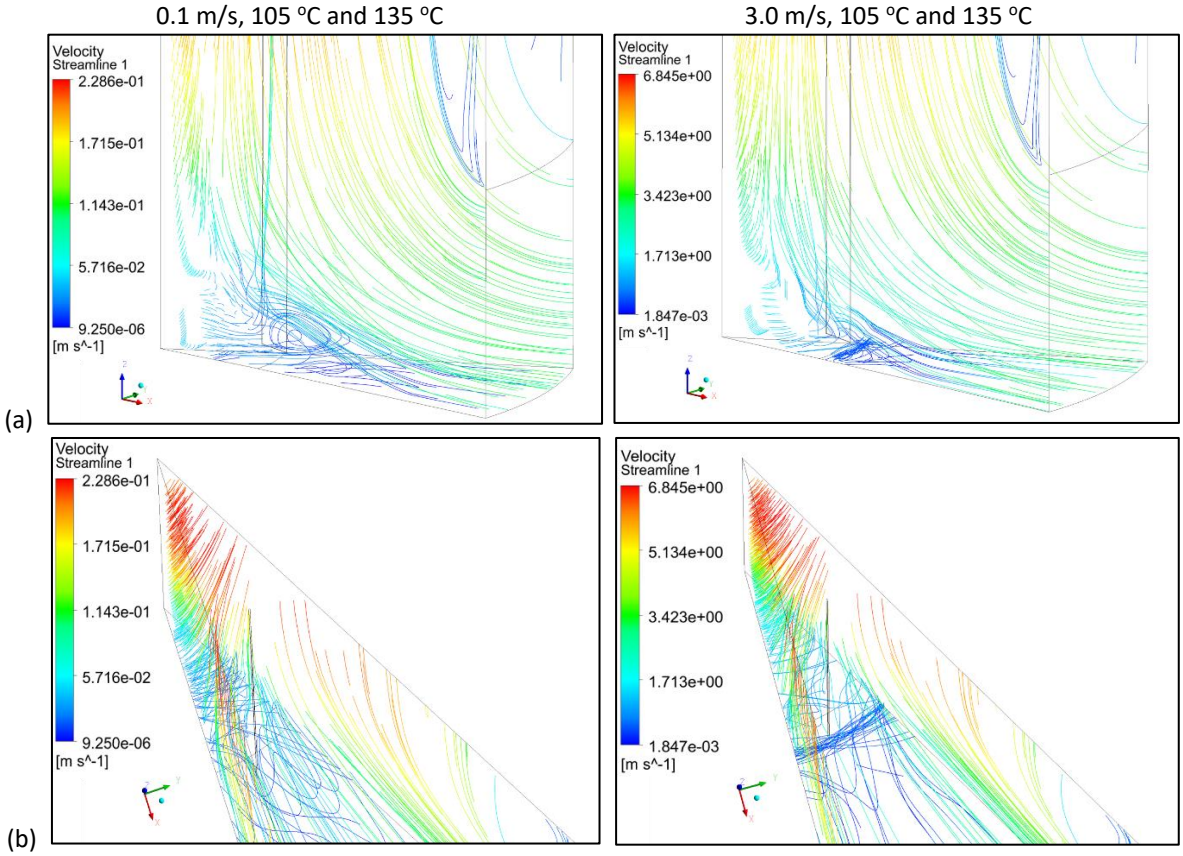

Figure 3. Streamlines projected from the left wedge surface, floor and heated plate viewed from (a) the left wedge face and (b) top of the domain. The streamlines are evenly spaced from their respective surfaces with 100 points per surface.

As shown in Figure 3, the modelled streamlines surrounding the floor, heated plate and vane reveal that the swirling flow at the boundary layer between these surfaces is stretched and tilted azimuthally, radially and axially in the anti-clockwise and upwards direction. This swirling flow then moves closer to the chamber axis and transitions into a vertical vortex that blends into the single-core vortex section 600 mm above the plate as the inlet radial velocity is increased from 0.1 m/s to 3.0 m/s, with increased localised u-, v- and w-velocities (with respect to the cartesian axes) above the plate that draw the heat away from the plate. The flow characteristics captured through the modelling is consistent with the MM statement that there is a vortex breakdown where the boundary layer erupts to produce the core flow vortex.

3.2 Mesh Refinement and Uncertainty Analysis

Discretisation error analysis based on the procedure specified in the Journal of Fluids Engineering Editorial Policy (ASME, 2008) was carried out to determine the level of uncertainty in (i) the two modelled ΔT values at 300 mm above the heated plate given their similarity with the experimental counterparts (at 0.1 m/s radial inlet velocity), and (ii) the level of uncertainty of the average vorticity values at 105 °C and 135 °C to determine if the different plate heat input values led to a significant effect on the average vorticity at 3.0 m/s radial inlet velocity. The flow calculations were run on three significantly different mesh grids with a grid refinement factor, *r*, of greater than 1.3, with the cell sizes being 0.0322 m for the coarse mesh, 0.0219 m for the medium mesh, and 0.0150 m for the fine mesh with a mean *r* of 1.466.

The ΔT at 300 mm above the 105 °C plate centre were 33.14 °C for the 0.0322 m mesh size, 33.41 °C for the 0.0219 m mesh size, and 34.00 °C for the 0.0150 m mesh size respectively. The apparent order of convergence, *p*, for the air temperature calculations was found to be 2.12, and a computation of

the scaled relative temperature error, defined by the grid convergence index (GCI), revealed a discretisation error of ± 0.017 °C for the fine 0.0150 m mesh and a more conservative discretisation error of ± 0.039 °C for the medium 0.0219 m mesh. The same calculations for the 135 °C plate setting also revealed a similar apparent order and discretisation error, and confirms the closeness of the calculated ΔT value of 46.69 ± 0.02 °C to the experimental result recorded in MM.

The apparent order for the average vorticity values above the plate at 105 °C and 135 °C was 1.59-1.60, and the vorticity values overlap each other: 193.88 ± 0.79 s^{-1} at 105 °C and 193.95 ± 0.79 s^{-1} at 135 °C using the fine meshes. It is therefore deemed that the different vorticity values at these temperatures are due to discretisation error rather than differences in heat input.

4. Conclusions

CFD modelling was carried out to attempt to replicate the single-cell buoyancy vortex experimental results obtained by Mullen and Maxworthy in 1977. The ANSYS-CFX model replicated the flow structure described by Mullen and Maxworthy as the swirling flow transitioned from the boundary layer at the floor, heated plate and vane into a vertical vortex and merged with the single-core vortex 600 mm above the plate. Mesh refinement and uncertainty analysis also revealed that the apparent order of convergence for the vortex core temperature was 2.12 and average vorticity was 1.59 - 1.60 across the 105°C and 135°C plate temperatures, and that the estimated uncertainty of the vortex core temperature values above ambient at 300 mm height was no higher than 0.02°C using the 0.0150 m fine meshes.

Acknowledgement

K.-W. Leong would like to express his gratitude for financial support from the University of Auckland Doctoral Scholarship.

References

American Society of Mechanical Engineers, (2008), Procedure for estimation and reporting of uncertainty due to discretization in CFD applications. *Journal of Fluids Engineering*. 130(7): 078001-1 – 078001-4. doi:10.1115/1.2960953

ANSYS, (2020), "Ansys Release 2020 R1", Canonsburg, Pennsylvania, USA.

Fitzjarrald, D.E. (1973), A laboratory simulation of convective vortices. *Journal of the Atmospheric Sciences*. 30(5): 894-902. doi:10.1175/1520-0469(1973)030<0894:ALSOCV>2.0.CO;2

Glezer, A., Simpson, M. (2014), U.S. Patent No. 8,875,509 B2. Washington, DC: U.S. Patent and Trademark Office.

Hawkes, N.A., Flay, R.G.J. (2016), Dust devil Heights and Windspeeds: A Modified Model. *18th Australasian Wind Engineering Society Workshop*, McLaren Vale, Australia, July 6-8, 2016.

Kaimal, J.C., Businger, J.A. (1970), Case studies of a convective plume and a dust devil. *Journal of Applied Meteorology and Climatology.* 9(4): 612-620. doi:10.1175/1520-0450(1970)009<0612:CSOACP>2.0.CO;2

Menter, F.R. (1994), Two-equation eddy-viscosity turbulence models for engineering applications. *AIAA Journal.* 32(8): 1598-1605. doi:10.2514/3.12149

Moukalled, F., Mangani, L., Darwish, M. (2016), "The finite volume method in computational fluid dynamics: An advanced introduction with OpenFOAM and Matlab": 69. doi:10.1007/978-3-319-16874-6

Mullen, J.B., Maxworthy, T. (1977), A laboratory model of dust devil vortices. *Dynamics of Atmospheres and Oceans.* 1(3): 181-214. doi:10.1016/0377-0265(77)90006-9

Nižetić, S. (2018). Carbon free electricity production from the alternative energy concepts based on the utilization of the convective vortex systems as a heat engines: Review of the current status and perspective. *Journal of Cleaner Production.* 170: 85-95. doi:10.1016/j.jclepro.2017.09.130

Simpson, M.W., Glezer, A. (2016), Buoyancy-induced, columnar vortices. *Journal of Fluid Mechanics.* 804: 712-748. doi:10.1017/jfm.2016.541

Stull, R.B. (2016), "Practical meteorology: an algebra-based survey of atmospheric science", 1.00b Edition, University of British Columbia, Vancouver: 497-498, 503, 587.